Final version published as: Kolappan, S., Shen, D. L., Mosi, R., Sun, J., McEachern, E. J., Vocadlo, D. J., & Craig, L. (2015). Structures of lactate dehydrogenase A (LDHA) in apo, ternary and inhibitor-bound forms. Acta Crystallographica Section D, 71(2), 185–195. https://doi.org/10.1107/S1399004714024791.

Acta Crystallographica Section D
Biological Crystallography
ISSN 1399-0047

Structures of lactate dehydrogenase A (LDHA) in apo, ternary and inhibitor-bound forms

Subramaniapillai Kolappan,[a] David L. Shen,[b] Renee Mosi,[b] Jianyu Sun,[b] Ernest J. McEachern,[b] David J. Vocadlo[a,b,c] and Lisa Craig[a]*

[a]Department of Molecular Biology and Biochemistry, Simon Fraser University, Burnaby, BC V5A 3Y6, Canada, [b]Alectos Therapeutics Inc., 8999 Nelson Way, Burnaby, BC V5A 4B5, Canada, and [c]Department of Chemistry, Simon Fraser University, Burnaby, BC V5A 1S6, Canada

Correspondence e-mail: licraig@sfu.ca

PDB references: LDHA, apo, 4ojn; complex with compound **1**, 4qt0; complex with compound **2**, 4qsm; complex with oxalate and NADH or kanamycin, 4okn

Lactate dehydrogenase (LDH) is an essential metabolic enzyme that catalyzes the interconversion of pyruvate and lactate using NADH/NAD^+ as a co-substrate. Many cancer cells exhibit a glycolytic phenotype known as the Warburg effect, in which elevated LDH levels enhance the conversion of glucose to lactate, making LDH an attractive therapeutic target for oncology. Two known inhibitors of the human muscle LDH isoform, LDHA, designated **1** and **2**, were selected, and their IC_{50} values were determined to be 14.4 ± 3.77 and $2.20 \pm 0.15\ \mu M$, respectively. The X-ray crystal structures of LDHA in complex with each inhibitor were determined; both inhibitors bind to a site overlapping with the NADH-binding site. Further, an apo LDHA crystal structure solved in a new space group is reported, as well as a complex with both NADH and the substrate analogue oxalate bound in seven of the eight molecules and an oxalate only bound in the eighth molecule in the asymmetric unit. In this latter structure, a kanamycin molecule is located in the inhibitor-binding site, thereby blocking NADH binding. These structures provide insights into LDHA enzyme mechanism and inhibition and a framework for structure-assisted drug design that may contribute to new cancer therapies.

1. Introduction

Lactate dehydrogenase (LDH) is an oxidoreductase enzyme that plays a central role in metabolism. LDH catalyzes the reversible conversion of the substrate pyruvate to lactate with the concomitant conversion of NADH, a 'co-substrate', to NAD^+. LDH, which is present in organisms ranging from bacteria to humans, is active as a tetramer. There are two major forms of LDH in humans: LDHA, encoded by the *LDHA* gene, is a homotetramer present in skeletal muscle (M4) and liver, and LDHB, encoded by the *LDHB* gene, is a homotetramer found in heart tissue (H4). The catalytic mechanism is conserved among isoforms and within species. First NADH and then pyruvate bind to an active-site cleft, inducing the closure of an active-site loop to seal the catalytic site from free solvent. Arg105 in the active-site loop clamps down on the bound pyruvate. A hydride ion is then transferred from the nicotinamide ring of NADH to the carbonyl O atom of pyruvate, with His193 acting as a catalytic general acid (Dunn *et al.*, 1991).

LDH has been implicated as a potential therapeutic target in oncology (Koukourakis *et al.*, 2003, 2005, 2006). Many tumours and cancer cells exhibit the Warburg effect, in which ATP is produced mainly *via* aerobic glycolysis, a metabolic pathway concluding with the LDH-catalyzed conversion of pyruvate to lactate (Vander Heiden, 2011; Warburg, 1956; Hamanaka & Chandel, 2012; Fantin *et al.*, 2006; Fiume *et al.*,

2010; Le *et al.*, 2010; Sheng *et al.*, 2012; Wang *et al.*, 2012; Xie *et al.*, 2009, 2014). Knockdown of LDHA by shRNA or inhibition by a small molecule results in oxidative damage and death of cancer cells (Granchi, Roy, Giacomelli *et al.*, 2011; Granchi, Roy, Mottinelli *et al.*, 2011). Thus, small-molecule LDH inhibitors are actively being sought to exploit this aberrant phenotype and block cancer-cell metabolism (Billiard *et al.*, 2013; Dragovich *et al.*, 2013, 2014; Fauber *et al.*, 2013; Granchi *et al.*, 2013; Kohlmann *et al.*, 2013; Carruthers *et al.*, 2012; Manerba *et al.*, 2012; Ward *et al.*, 2012; Yang *et al.*, 2014).

Atomic structures of LDH have informed catalytic mechanism and provide a foundation for the design of inhibitory molecules as potential anticancer therapeutics. Only a few apo LDH structures from eukaryotes have been reported to date: LDH M4 from dogfish (PDB entry 6ldh; Abad-Zapatero *et al.*, 1987), LDH C4 from mouse testes (PDB entry 2ldx; Hogrefe *et al.*, 1987) and, most recently, human muscle LDHA (PDB entry 4l4r; Dempster *et al.*, 2014). Most of the apo LDHA structures have an open conformation of the active site, in which the mobile active-site loop, residues ∼95–110, is oriented away from the body of the enzyme, allowing free diffusion of substrate and co-substrate into the extended ligand-binding groove. An exception is the mouse apo LDH C4 structure, in which the active-site loop is closed in each of the four molecules in the tetrameric asymmetric unit (PDB entry 2ldx; Hogrefe *et al.*, 1987). Just as the apo structure is not always crystallized in an open conformation, the presence of ligand in the active site does not necessarily result in closure. NADH-bound human LDHA structures have an open conformation (PDB entry 4l4s; Dempster *et al.*, 2014), and ternary complexes with NADH and the pyruvate analogue oxamate can be closed, as in the octameric asymmetric unit of pig LDH (PDB entries 9ldb and 9ldt; Dunn *et al.*, 1991), or a combination of open and closed forms, as in the human and rabbit LDHA ternary structures (PDB entries 1i10 and 3h3f; Read *et al.*, 2001; Swiderek *et al.*, 2009). Collectively, these structural variations suggest that (i) ligand binding can occur without active-site loop closure and that (ii) the active-site loop is dynamic and switches between the open and closed conformation both in the absence and the presence of ligand.

A number of crystal structures have been reported for mammalian LDH in complex with small-molecule inhibitors identified by screening compound libraries (Dragovich *et al.*, 2013; Fauber *et al.*, 2013; Kohlmann *et al.*, 2013; Ward *et al.*, 2012). These include pyrazine-based and pyrimidine-based inhibitors that bind in the active-site cleft simultaneously with NADH co-substrate (Dragovich *et al.*, 2013; Fauber *et al.*, 2013), and those designed to span the active site using a fragment-based drug-discovery approach (Kohlmann *et al.*, 2013; Ward *et al.*, 2012). As part of our interest in developing LDHA inhibitors to modulate cancer-cell metabolism, we characterized two known quinoline-based inhibitors of human LDHA (Chai *et al.*, 2012) and obtained X-ray crystal structures of the LDHA–inhibitor complexes. We also report a new apo LDHA structure solved in a different space group to that reported previously (Dempster *et al.*, 2014) plus a ternary complex with NADH and the substrate analogue oxalate, in which the NADH in one of the eight molecules in the asymmetric unit is replaced by kanamycin. We discuss the implications of these structures for enzyme mechanism and inhibitor design.

2. Materials and methods

2.1. Cloning and expression of LDHA

The human *LDHA* gene encoding a C-terminal hexahistidine tag was synthesized by GeneArt (Life Technologies) based on GenBank locus CAG46515 with codon usage adapted to *Escherichia coli*. The gene was inserted into the pET-29b expression vector (Novagen) using *Nde*I/*Xho*I sites, which results in a His tag appended to the C-terminus of LDHA. The gene sequence was verified and the resulting pET-29b-*LDHA* vector was introduced into *E. coli* BL21(λDE3) cells (Stratagene) by transformation following the manufacturer's protocol. Cells containing the *LDHA* vector were selected by overnight growth on Luria–Bertani (LB) agar plates containing 50 µg ml^{-1} kanamycin at 37°C. A single colony was picked from the plate and grown at 37°C overnight in LB broth containing 50 µg ml^{-1} kanamycin (LB-kan) to obtain a starter culture. A 10 ml aliquot of the starter culture was introduced into 1 l LB-kan and grown at 37°C with shaking to an optical density of between 0.6 and 1 at 600 nm. Protein expression was induced with 0.025 m*M* isopropyl β-D-1-thiogalactopyranoside (IPTG) and the cells were grown for a further 23 h at room temperature. The cells were harvested by centrifugation (4960*g*, 10 min, 4°C) and stored as a pellet at −80°C until use.

2.2. LDHA purification

Frozen cell pellets from 2 l culture were suspended in buffer *A* (20 m*M* NaH_2PO_4/Na_2HPO_4 pH 7.5, 100 m*M* NaCl) plus protease-inhibitor cocktail tablets (EDTA-free, Roche). Lysozyme was added to a final concentration of 2 mg ml^{-1} and the suspension was gently stirred at room temperature for 1 h followed by sonication to lyse the cells. Intact cells and insoluble material were removed by centrifugation at 40 000*g* and 4°C for 60 min. The supernatant was filtered using a 0.4 µm membrane and loaded onto an Ni–NTA column pre-equilibrated with buffer *A* containing 30 m*M* imidazole. The Ni–NTA column was washed with 20 column volumes of buffer *A* and the protein was eluted with 300 m*M* imidazole pH 7.5 in buffer *A*. The eluted protein was dialyzed exhaustively in 100 m*M* HEPES pH 7.5 and centrifuged at 5000*g* and 4°C for 30 min to remove insoluble material. The protein was concentrated using an Amicon Ultra-15 filter unit (10 000 Da molecular mass cutoff, Millipore) and further purified using a HiPrep 16/60 Sephacryl S-300 HR size-exclusion column (GE Life Sciences) pre-equilibrated with 100 m*M* HEPES pH 7.5. LDHA eluted as a tetramer and was estimated by SDS–PAGE to be greater than 95% pure. LDHA was concentrated to 25 mg ml^{-1} using an Amicon Ultra-15 filter with a 10 000 Da

Table 1
Data-collection and refinement statistics for LDHA structures.

Values in parentheses are for the last shell.

	Apo LDHA	LDHA–oxl–NADH/kan	LDHA–**1**	LDHA–**2**
Data statistics				
Beamline	SSRL 7-1	SSRL 7-1	SSRL 7-1	SSRL 7-1
Wavelength (Å)	1.0	1.0	1.0	1.0
Space group	$P3_121$	$P2_12_12_1$	$P3_121$	$P3_121$
a, b, c (Å)	147.1, 147.1, 333.2	65.6, 159.6, 266.2	147.2, 147.2, 334.6	147.3, 147.3, 334.5
α, β, γ (°)	90.0, 90.0, 120.0	90.0, 90.0, 90.0	90.0, 90.0, 120.0	90.0, 90.0, 120.0
Resolution (Å)	2.4	2.1	3.2	3.0
Completeness (%)	99.5 (97.2)	99.9 (100.0)	99.6 (100)	99.9 (99.9)
No. of observed reflections	1175796	898093	515938	629385
No. of unique reflections	162753	163531	69933	84925
$R_{\rm p.i.m.}$† (%)	8.6 (64.2)	9.9 (82.1)	7.0 (48.0)	5.8 (39.8)
$\langle I/\sigma(I)\rangle$	22.8 (2.9)	14.4 (2.1)	13.7 (1.9)	14.6 (2.2)
Wilson B value (Å^2)	44.0	37.7	57.9	52.1
Refinement statistics				
Resolution limits (Å)	20.0–2.4	34.0–2.1	35.0–3.2	35.0–3.0
Z	48	32	48	48
No. of reflections used	154614	155268	66105	80339
$R_{\rm cryst}$‡ (%)	21.3	20.6	17.2	16.7
$R_{\rm free}$§ (%)	25.0	24.5	27.1	24.7
No. of atoms				
Protein	21083	20544	21017	20814
Ligands	146	434	264	272
Water	527	775	24	60
Average B factor (Å^2)				
Protein				
Chain *A*	30.5	28.8	65.3	61.2
Chain *B*	28.8	28.1	75.1	63.6
Chain *C*	28.4	25.9	65.0	60.7
Chain *D*	29.2	23.7	68.8	60.9
Chain *E*	36.1	28.9	87.0	81.3
Chain *F*	28.2	30.4	70.3	65.7
Chain *G*	25.3	29.6	67.9	61.0
Chain *H*	32.3	35.0	79.7	73.2
Ligands				
Glycerol	58.6	—	—	—
PEG 400	45.9	—	—	—
NADH	—	31.0	—	—
Oxalate	—	28.3	—	—
Sulfate	—	42.4	—	—
Kanamycin	—	62.9	—	—
1	—	—	67.8	—
2	—	—	—	66.2
Water oxygen	32.5	33.6	47.5	47.0
R.m.s.d., bond lengths (Å)	0.008	0.007	0.014	0.011
R.m.s.d., bond angles (°)	1.32	1.27	1.78	1.55
Ramachandran plot				
Favoured (%)	97.6	97.3	92.2	95.7
Allowed (%)	2.1	2.5	6.8	3.8
Outlier (%)	0.2	0.2	1.0	0.5
PDB code	4ojn	4okn	4qt0	4qsm

† $R_{\rm p.i.m.} = \sum_{hkl}\{1/[N(hkl)-1]\}^{1/2}\sum_i |I_i(hkl) - \langle I(hkl)\rangle|/\sum_{hkl}\sum_i I_i(hkl)$. ‡ $R_{\rm cryst} = \sum_{hkl}||F_{\rm obs}| - |F_{\rm calc}||/\sum_{hkl}|F_{\rm obs}|$. § $R_{\rm free}$ is the cross-validation R factor for 5% of the reflections against which the model was not refined.

molecular-mass cutoff membrane, flash-frozen in liquid nitrogen and stored at −80°C.

2.3. Inhibitor synthesis

3-{[3-Carbamoyldimethoxypyrimidin-7-(2,4-dimethoxypyrimidin-5-yl)quinolin-4-yl]amino}benzoic acid (compound **1**) and 3-{[7-(2,4-dimethoxypyrimidin-5-yl)-3-sulfamoylquinolin-4-yl]aminobenzoic acid (compound **2**) were prepared according to the procedures reported by Chai *et al.* (2012).

2.4. Inhibition assays

2.4.1. Absorbance assay. Compounds **1** and **2** were dissolved at 20 m*M* in dimethyl sulfoxide (DMSO) and working stocks were prepared in assay buffer [phosphate-buffered saline (PBS) containing 0.001% Triton and 20%(*v*/*v*) DMSO] through serial dilution. Assay buffer was added to wells of a standard 96-well assay plate stamped with NADH and LDHA (final concentrations: 500 µ*M* NADH, 1 n*M* LDHA) and incubated for 5 min at room temperature. Inhibitor solutions were added to all wells (final DMSO content: 2%) and the mixtures were incubated for 5 min at room temperature. A solution of pyruvate (final concentration: 1 m*M*) was added to each well and the consumption of NADH was monitored through the decrease in absorbance (340 nm) over 10 min at 37°C using a Molecular Devices SpectraMax 250 reader. The $K_{\rm i}$ values for compound **2** were determined using the same procedure with fixed inhibitor concentrations ranging between 0 and 2.5 µ*M*, and pyruvate or NADH were varied in a systematic fashion. The mode of inhibition was determined by using a Lineweaver–Burk plot to display the data, and the $K_{\rm i}$ value was obtained using *GraphPad Prism* to obtain the best fit.

2.4.2. Fluorescent assay. Inhibitor dilutions were prepared as described for the absorbance assay. Assay buffer was added to one column (n = 3) of a standard 96-well plate containing inhibitor solutions (final DMSO content: 2%). LDHA and NAD^+ in assay buffer (final concentrations: 300 p*M* LDHA and 150 µ*M* NAD^+) were added to the remaining wells and the mixtures were incubated for 10 min at room temperature. A solution of lactate, resazurin and diaphorase (final concentrations: 0.2 m*M* lactate, 0.625 µ*M* resazurin, 0.04 U ml^{-1} diaphorase) in assay buffer was added to all wells and the mixtures were incubated for 30 min at room temperature. Stop solution (25 m*M* oxamate in assay buffer) was added to each well and the fluorescence intensity was measured at 571 nm (excitation)/590 nm (emission) on a BioTek Synergy H4 reader.

2.5. Protein crystallization

LDHA crystals were grown by the hanging-drop vapour-diffusion method at 20°C. Initial crystallization conditions

were obtained from the high-throughput screening laboratory at the Hauptman–Woodward Medical Research Institute (Luft *et al.*, 2003). Apo LDHA crystals were grown by mixing 2 µl 25 mg ml^{-1} LDHA with 2 µl reservoir solution consisting of 100 m*M* bis-tris propane pH 7.0, 20%(*v*/*v*) PEG 400, 100 m*M* LiCl. LDHA–NADH crystals were grown by first incubating 25 mg ml^{-1} LDHA with NADH (3 m*M*) for 2 h at 4°C and then setting up 4 µl drops with a 2:1:1 volume ratio of LDHA–NADH, reservoir solution [18%(*w*/*v*) PEG 3350, 50 m*M* HEPES pH 6.8] and Silver Bullets Bio Screen 1 reagent A1 [Hampton Research; 0.16%(*w*/*v*) L-citrulline, 0.16%(*w*/*v*) L-ornithine hydrochloride, 0.16%(*w*/*v*) urea, 0.16%(*w*/*v*) oxalic acid, 0.16%(*w*/*v*) kanamycin monosulfate, 0.16%(*w*/*v*) L-arginine, 0.02 *M* HEPES sodium pH 6.8]. The oxalate and kanamycin found in the LDHA ternary complex were derived from reagent A1. Apo and NADH-bound LDHA crystals appeared after three weeks. LDHA–inhibitor complex crystals were obtained by adding 10 µl soaking solution [20 m*M* inhibitor, 100 m*M* HEPES pH 7.5, 50 m*M* LiCl, 100 m*M* bis-tris propane pH 7.0, 20%(*v*/*v*) DMSO, 25% PEG 8000] to 2 µl hanging drops containing apo LDHA crystals and allowing the crystals to sit at room temperature

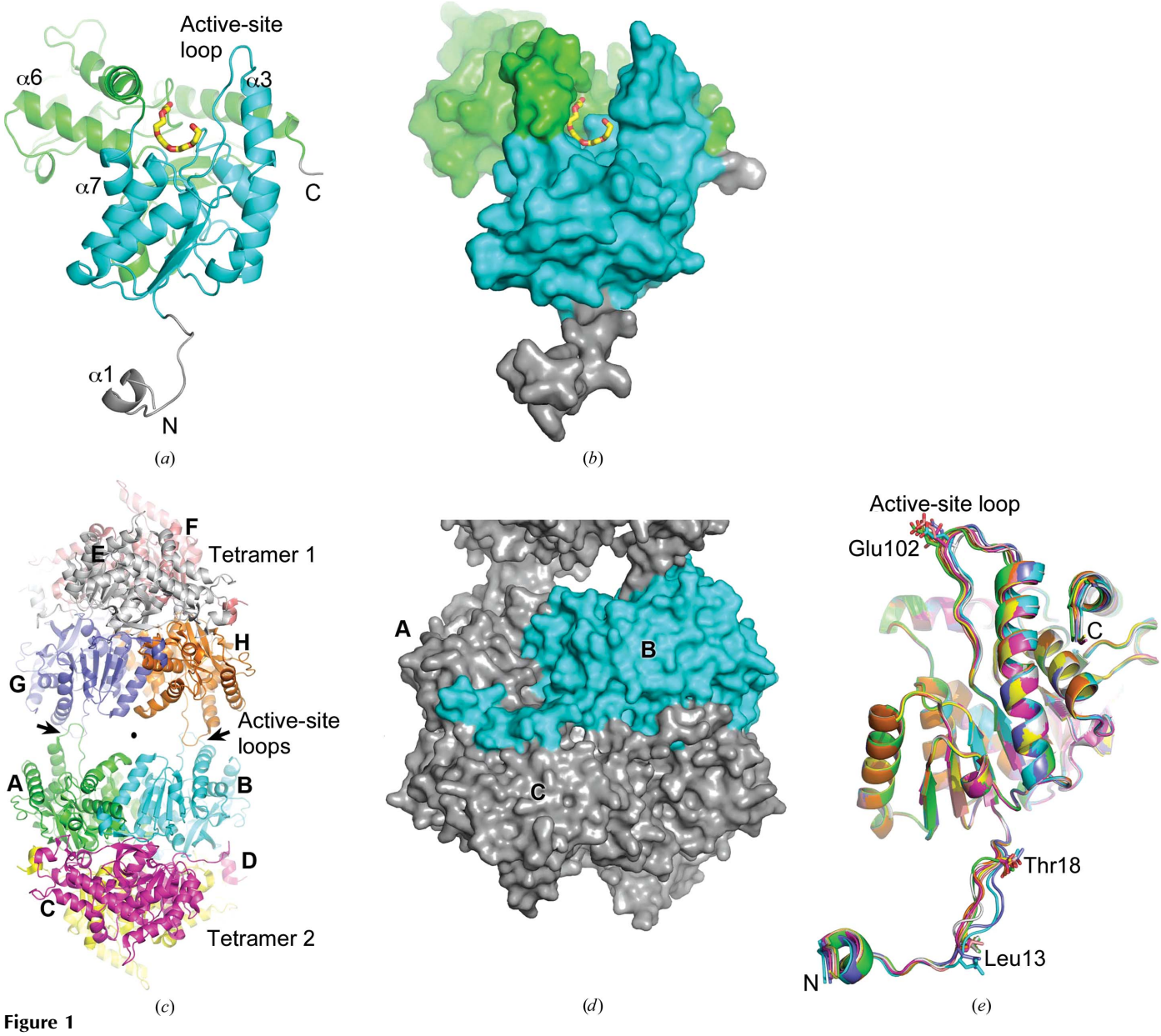

Figure 1
Human apo LDHA structure. (*a*) Apo LDHA chain *A* is shown in (*a*) cartoon and (*b*) surface representations, with the extended N-terminus coloured grey and the large and small domains coloured cyan and green, respectively. The active-site cleft is framed by α6 and the α6–α7 loop on the small domain side and by the active-site loop between β4 and α3 on the large domain side. The polyethylene glycol 400 (PEG) molecule is shown in stick representation with its C atoms coloured yellow and its O atoms coloured red. (*c*) The apo LDHA octamer, which is a dimer of tetramers joined by interactions between the active-site loops of chains *A* and *G* and chains *B* and *H*. The twofold symmetry axis is indicated with a black spot. (*d*) Space-filling representation of the apo LDHA octamer chain *B* coloured cyan to shown the extended conformation at the N-terminus. (*e*) Superposition of the eight molecules in the asymmetric unit of the apo LDHA structure. The maximum r.m.s.d. between each chain and chain *A* is 0.65 Å (main-chain atoms).

for 24 h. All crystals were cryocooled in liquid nitrogen for storage and transport to the Stanford Synchrotron Radiation Lightsource (SSRL) for X-ray diffraction data collection.

2.6. Data collection, processing and structure determination

X-ray diffraction data for LDHA crystals were collected at 100 K on beamline 7-1 at SSRL using the *Blu-Ice* software (González *et al.*, 2008). The raw data were processed, integrated and scaled using *XDS* (Kabsch, 2010). Matthews coefficient calculations (Matthews, 1968) indicated that all crystals contained eight molecules in the asymmetric unit, with water contents of 65% for apo LDHA, 46% for LDHA–NADH and 65% for the complexes of LDHA with both compound **1** (LDHA–**1**) and compound **2** (LDHA–**2**). Structures were determined by the molecular-replacement method using *Phaser* (McCoy *et al.*, 2007) and refined using *REFMAC* (Murshudov *et al.*, 2011) in the *CCP*4 suite (Winn *et al.*, 2011). The apo LDHA structure was solved using the structure of human LDHA in complex with NADH and oxamate (PDB entry 1i10; Read *et al.*, 2001) as the search model. *Phaser* gave two unique solutions with high *Z*-scores. Several cycles of rigid-body refinement were performed followed by refinement with noncrystallographic symmetry restraints using *REFMAC*. Difference maps were generated and inspected in *Coot* (Emsley & Cowtan, 2004), clearly indicating a conformational difference in the active-site loop in the apo structure relative to the search model PDB entry 1i10. Iterative cycles of model building and refinement using *REFMAC* and *Coot* improved the model and reduced the *R* values. Water O atoms and ligands were located in *Coot* and verified by a composite annealed OMIT map using the *CNS* suite of programs (Brünger *et al.*, 1998). The final 2.4 Å resolution structure, which has an $R_{\rm cryst}$ of 0.213 and an $R_{\rm free}$ of 0.250, was validated using *PROCHECK* (Laskowski *et al.*, 1993) and *MolProbity* (Chen *et al.*, 2010) (Table 1). The amino-acid sequence of LDHA is numbered according to GenBank locus CAG46515.

A tetramer of the apo LDHA structure was used as a model to solve the LDHA–NADH complex by molecular replacement, yielding two solutions with *Z*-scores of 11.2 and 9.7.

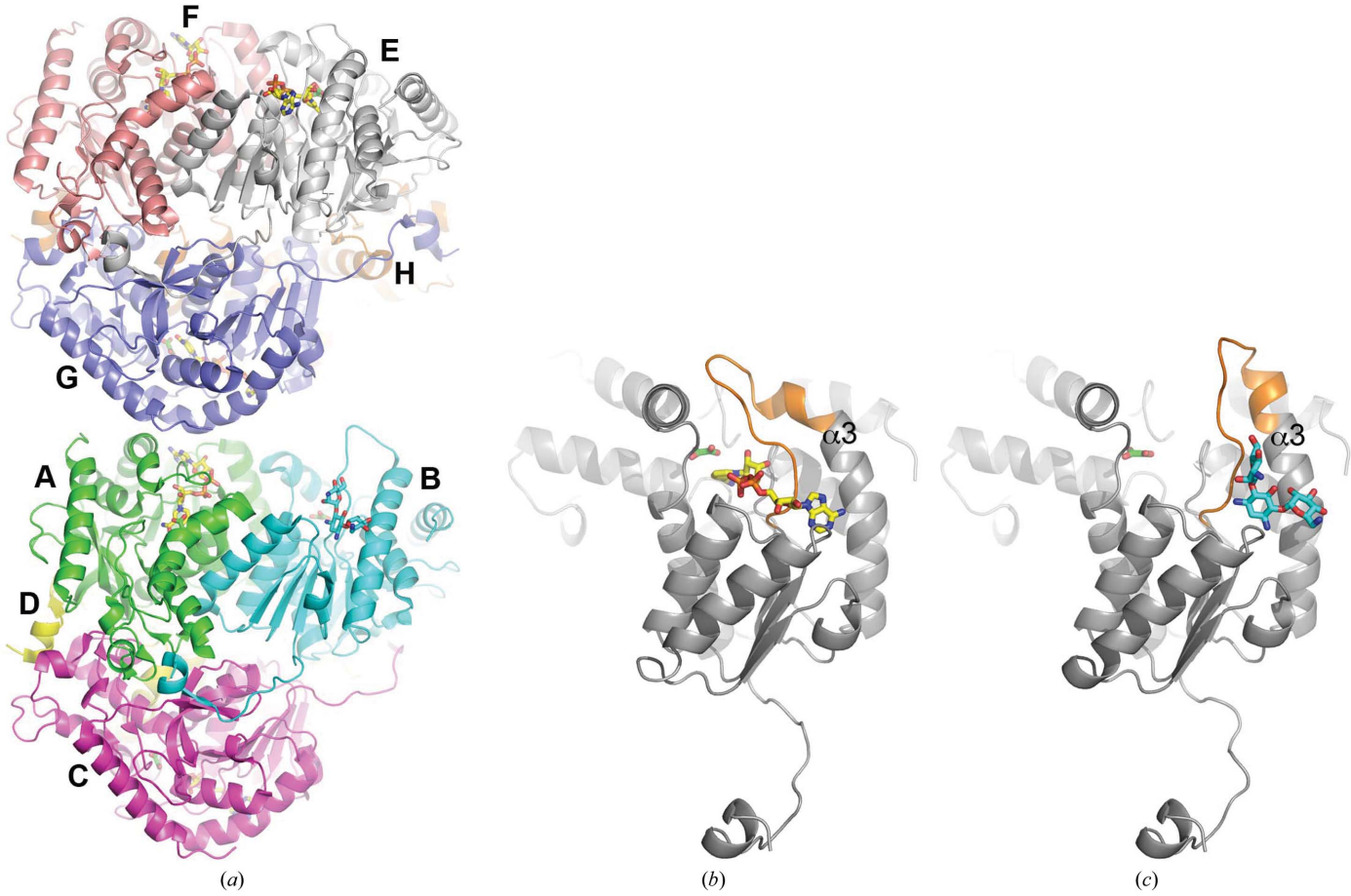

Figure 2
Ternary LDHA crystal structures. (*a*) The ternary LDHA octamer, which is a dimer of tetramers joined by interactions between the closed active-site loops of chains *A* and *G*. Chains *A*, *C*, *D*, *E*, *F*, *G* and *H* have oxalate and NADH bound in the active site, while chain *B* has oxalate and kanamycin. LDHA molecules are shown in cartoon representation and coloured by chain; ligands are shown as sticks with oxalate C atoms coloured green, NADH C atoms coloured yellow and kanamycin C atoms coloured cyan. For all ligands, N atoms are coloured blue, O atoms are red and phosphates are orange. (*b*) Closed chain *A* with oxalate (green C atoms) and NADH (yellow C atoms) and (*c*) open chain *B* with oxalate (green C atoms) and kanamycin (cyan C atoms). LDHA is coloured grey with its active-site loop shown in orange.

After a few cycles of restrained refinement, the difference maps were examined in *Coot* (Emsley & Cowtan, 2004), revealing structural changes in the active-site loop relative to apo LDHA and positive electron density for NADH in the active sites of seven of the eight monomers in the asymmetric unit. In addition, positive electron density matching oxalate was found in all eight monomers. The active-site loop was rebuilt using *Coot* (Emsley & Cowtan, 2004). After several further cycles of restrained refinement, water O atoms were located and the structures were further refined. The final structure, which has a resolution of 2.1 Å, an $R_{\rm cryst}$ of 0.206 and an $R_{\rm free}$ of 0.245, was validated using *PROCHECK* and *MolProbity* (Laskowski *et al.*, 1993; Chen *et al.*, 2010; Table 1).

The apo LDHA tetramer was also used as a molecular-replacement model for the LDHA–inhibitor structures. After a few cycles of rigid-body refinement followed by further cycles of restrained refinement with medium noncrystallographic symmetry restraints (NCS) restraints, weighted 'difference' maps ($mF_{\rm obs} - DF_{\rm calc}$) were calculated. Difference maps contoured at 3.0σ had density near the active-site mobile loop, indicating the presence of inhibitor, in each of the eight molecules in the asymmetric units of LDHA–**1** and LDHA–**2**. For refinement, *SKETCHER* in the *CCP*4 suite was used to create inhibitor library descriptions. After iterative cycles of restrained refinement, model adjustments and water location, the complex structures were validated by *PROCHECK* and *MolProbity* (Table 1). The final LDHA–**1** structure has a resolution of 3.2 Å and $R_{\rm cryst}$ and $R_{\rm free}$ values of 0.172 and 0.271, respectively. The LDHA–**2** structure has a resolution of 3.0 Å and $R_{\rm cryst}$ and $R_{\rm free}$ values of 0.167 and 0.247, respectively.

3. Results

3.1. Human apo LDHA crystal structure

The human apo LDHA structure was solved at 2.4 Å resolution. Apo LDHA crystallized in space group $P3_121$ with eight molecules in the asymmetric unit. The structure is essentially identical to the recently published apo LDHA structure (PDB entry 4l4r; Dempster *et al.*, 2014), which crystallized in space group $P4_122$ with two molecules per asymmetric unit. The 332-residue human LDHA is a globular protein of mixed α/β secondary structure with a protruding N-terminal segment (Figs. 1*a* and 1*b*). The LDHA active site lies in an extended groove between two domains: a larger 'co-substrate-binding' domain that has a Rossmann-type fold and a smaller 'substrate-binding' domain. The active-site loop (residues 95–110) is in an open conformation.

Although these LDHA structures lack bound substrate and co-substrate, they are not *bona fide* apo structures owing to the presence of a polyethylene glycol (PEG 400), derived from the crystallization conditions, in the active site of all eight molecules (Figs. 1*a* and 1*b*). PEG 400 fits in a C-shape into the active site, with its ends pointing outwards. Three of the PEG 400 O atoms are positioned to hydrogen bond to Asp138 $N^{\delta2}$ and the remainder of its interactions with LDHA are hydrophobic. This molecule lies adjacent to the substrate-binding site and overlaps with the NADH nicotinamide-binding site. The presence of PEG 400 in the active site appears to have no effect on the LDHA structure, which matches the published apo LDHA structure with PDB code 4l4r [Dempster *et al.*, 2014; root-mean-square deviation (r.m.s.d.) of 0.46 Å for backbone atoms of chain *A*].

Apo LDHA crystallized as a dimer of tetramers, with the monomers within each tetramer

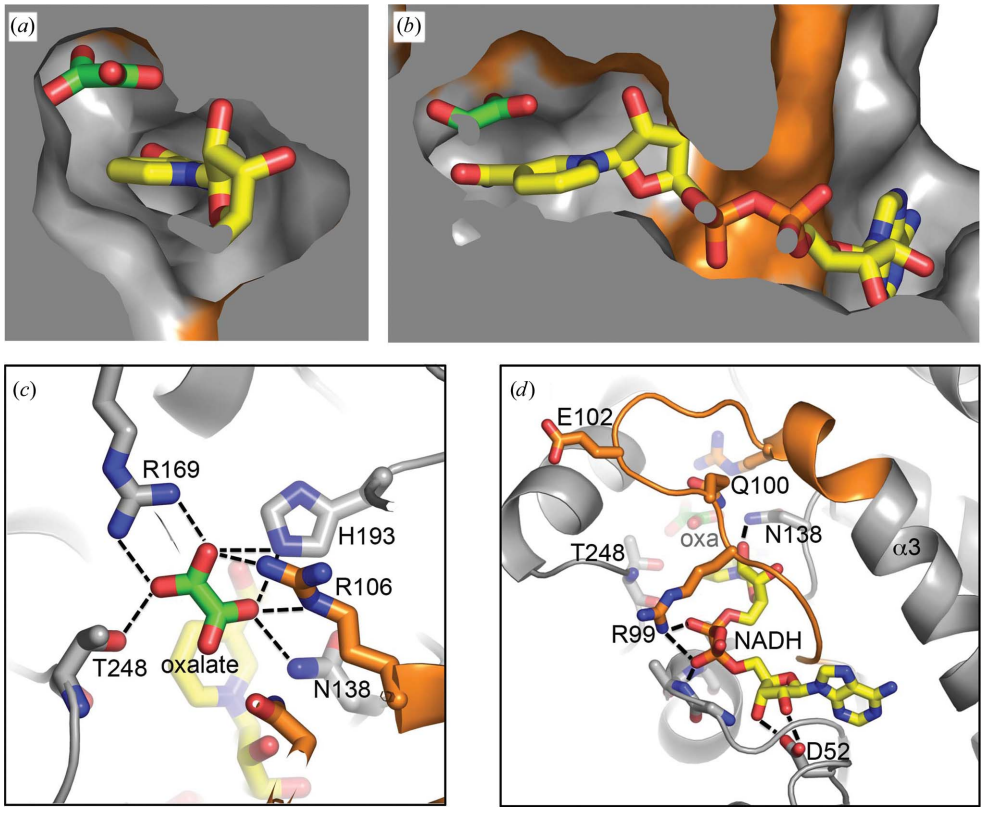

Figure 3
Interactions of oxalate and NADH in the ternary LDHA complex. (*a, b*) Solvent-excluded tunnel with oxalate and NADH bound shown in two different views. LDHA is shown in grey space-filling representation with its active-site loop coloured orange. Ligands are shown in stick representation, with oxalate C atoms coloured green, NADH C atoms yellow, N atoms blue, O atoms red and phosphates orange. (*c*) Interactions between oxalate and the LDHA substrate-binding site. Interacting side chains are shown in stick representation. (*d*) Interactions between NADH and the co-substrate-binding site.

related by 222 symmetry and the two tetramers related by twofold symmetry (Fig. 1*c*). Within each tetramer, the extended N-terminus of each monomer makes pairwise interactions with two adjacent molecules (Fig. 1*d*). All eight molecules in the asymmetric unit are very similar in structure, superimposing with a maximum r.m.s.d. of 0.69 Å for main-chain atoms. Minor structural variations occur in the N-terminal extensions between residues 13 and 18, and in the active-site loops, which differ by as much as 2.8 Å for the C^{α} positions of Glu102 at the apex of the loop (Fig. 1*e*). The active-site loops mediate the only contacts between the two tetramers in the asymmetric unit: the active-site loop of chain *A* in tetramer 1 hydrogen bonds to that of chain *G* in tetramer 2, and reciprocal interactions are observed between chain *H* in tetramer 2 and chain *B* in tetramer 1 (Fig. 1*c*). Glu102 of chains *A* and *H* penetrates the active-site grooves of chains *G* and *B*, respectively, but is oriented away from its partners for chains *G* and *B*. Corresponding interactions occur between chains *C* and *E* and chains *D* and *F* to link adjacent asymmetric units in the crystal lattice.

3.2. Human LDHA ternary structures

In an attempt to determine a binary structure, we co-crystallized LDHA with NADH and solved its structure to 2.1 Å resolution in space group $P2_12_12_1$. As with our apo LDHA structure, the LDHA–NADH complex is a dimer of tetramers (Fig. 2*a*). Electron density consistent with NADH was present in the co-substrate-binding sites of seven of the eight molecules (Fig. 2*b*). All eight molecules also had additional density in the substrate-binding pocket consistent with oxalate (oxl), a nonreactive analogue of the natural substrate pyruvate, in which the methyl ketone group of pyruvate is replaced by a carboxylate moiety (Figs. 2*b* and 2*c*). While oxalate was not explicitly included in the crystallization setup, it is present in reagent A1 of the Silver Bullets Bio Screen 1 (Hampton Research). Thus, seven of the eight molecules represent ternary structures that closely match the published ternary structures of human LDHA in complex with NADH and oxamate (PDB entry 1i10; Read *et al.*, 2001), which also crystallized in space group $P2_12_12_1$. The active-site loop is closed in each of these molecules. No NADH is present in the eighth LDHA molecule (chain *B*), but a kanamycin molecule (kan) is bound near the active-site loop, overlapping with the NADH-binding site (Fig. 2*c*). In contrast to the closed LDHA–oxl–NADH structures, the LDHA–oxl–kan structure is in an open conformation.

The subunit–subunit interactions within each tetramer are almost identical to those seen for the apo LDHA tetramers. However, the closed conformation for seven of the eight molecules results in an asymmetric octamer in which the two tetramers are tilted relative to each other and connected by only two chains: *A* and *G* (Fig. 2*a*).

The closed conformation in the LDHA–oxl–NADH structures seals the binding-site cleft at the substrate-binding end, creating a narrow tunnel-like cavity in which the planar oxalate is buried at the far end and the NADH nicotinamide moiety is wedged tightly between the oxalate and the floor of the active-site cavity (Figs. 3*a* and 3*b*). The pyrophosphate unit and adenosine moiety of NADH are located at the opening of the cavity. The interactions between substrate, co-substrate and LDHA have been described in detail

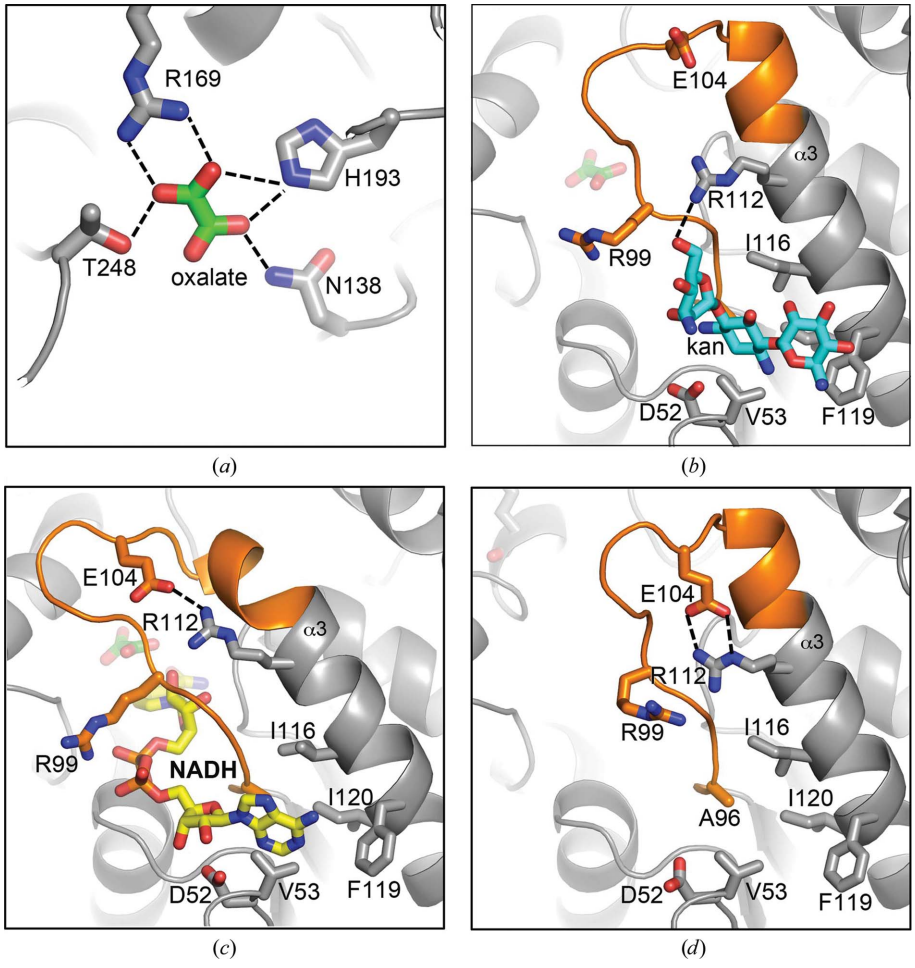

Figure 4
Interactions of oxalate and kanamycin in chain *B* of the ternary LDHA complex. (*a*) Close-up of oxalate in the substrate-binding site. (*b*) Close-up of bound kanamycin. The corresponding sites in (*c*) the ternary LDHA–oxl–NADH complex and (*d*) apo LDHA are shown for comparison. LDHA is shown in a grey cartoon representation with its active-site loop coloured orange. Interacting side chains are shown in stick representation, as are the ligands, with oxalate C atoms coloured green and kanamycin C atoms coloured cyan. N atoms are shown in blue, O atoms in red and phosphates in orange.

elsewhere (Dunn *et al.*, 1991; Dempster *et al.*, 2014). Briefly, oxalate is held in the substrate-binding pocket by an extensive network of planar hydrogen bonds and electrostatic contacts to Asn138, Arg169, His193 and Thr248 (Fig. 3*c*). Arg106 at the tip of the closed active-site loop clamps down on oxalate. The nicotinamide ring of NADH stacks with the oxalate and hydrogen-bonds to Asn138, Gln100, Ser161 and His193 (Fig. 3*d*). The side chain of the active-site loop residue Arg99 reaches across the active-site cleft, with its NH1 hydrogen bonding to the NADH pyrophosphate. The NADH adenosine lies in a hydrophobic pocket at the solvent-exposed end of the closed active site, with its 2′- and 3′-hydroxyl groups hydrogen-bonded to the side-chain carboxylate of Asp52.

Chain *B* of the ternary complex, which lacks NADH, is highly similar to the NADH-bound chains, differing only in having an open conformation (Figs. 2*b* and 2*c*). The oxalate lies in the same position and shares the same planar hydrogen-bond network as seen in the other seven molecules in the asymmetric unit, with the exception of the missing Arg106 clamp, which requires a closed active site to engage (Fig. 4*a*). Kanamycin is bound in a V-shape in the hydrophobic pocket at the open end of the active-site groove, with its central aminocyclohexyl ring penetrating the groove (Fig. 4*b*) and overlapping with the adenine-binding site of NADH (Fig. 4*c*) and its two flanking glycans pointing outwards. Kanamycin, which, like oxalate, originated from the Silver Bullet crystallization solution, is not as well resolved as the oxalate and NADH ligands. Only minor alterations in side-chain conformation accompany kanamycin binding, as the structure of chain *B* is almost identical to that of the apo LDHA structure (Fig. 4*d*). Arg99 swings away to make room for the kanamycin hydroxymethyl glucopyranose ring and Arg112 hydrogen-bonds to one of the hydroxyl groups on this ring, disrupting the Arg112–Glu104 salt bridge seen in the apo LDHA structure. Several hydrophobic side chains contact kanamycin, but their conformations are also unchanged relative to the apo structure. These include α3 helix residues Ile116, Ile120 and Phe119, the phenyl ring of which stacks with the aminomethyl glucopyranose ring of kanamycin. Thus, kanamycin binds to a highly complementary site on LDHA and is likely to prevent access of NADH by blocking the adenine-binding site.

3.3. Characterization of LDHA inhibitors

The two known inhibitors, compounds **1** and **2**, were analyzed for their ability to inhibit LDHA by measuring the decrease in absorbance as NADH is converted to NAD^+ upon LDHA-catalyzed conversion of pyruvate to lactate. As shown in Fig. 5(*a*), compounds **1** and **2** inhibit LDHA activity moderately, with IC_{50} values of 14.4 $\pm$ 3.77 and 2.20 $\pm$ 0.15 μM, respectively (Fig. 5*a*). The inhibition was also assayed in the reverse direction of catalysis (with lactate as the substrate) using a fluorescent-based coupled assay, which gave IC_{50} values of 0.51 $\pm$ 0.14 μM for compound **1** and 0.039 $\pm$ 0.007 μM for compound **2** (Fig. 5*b*). K_i values were determined

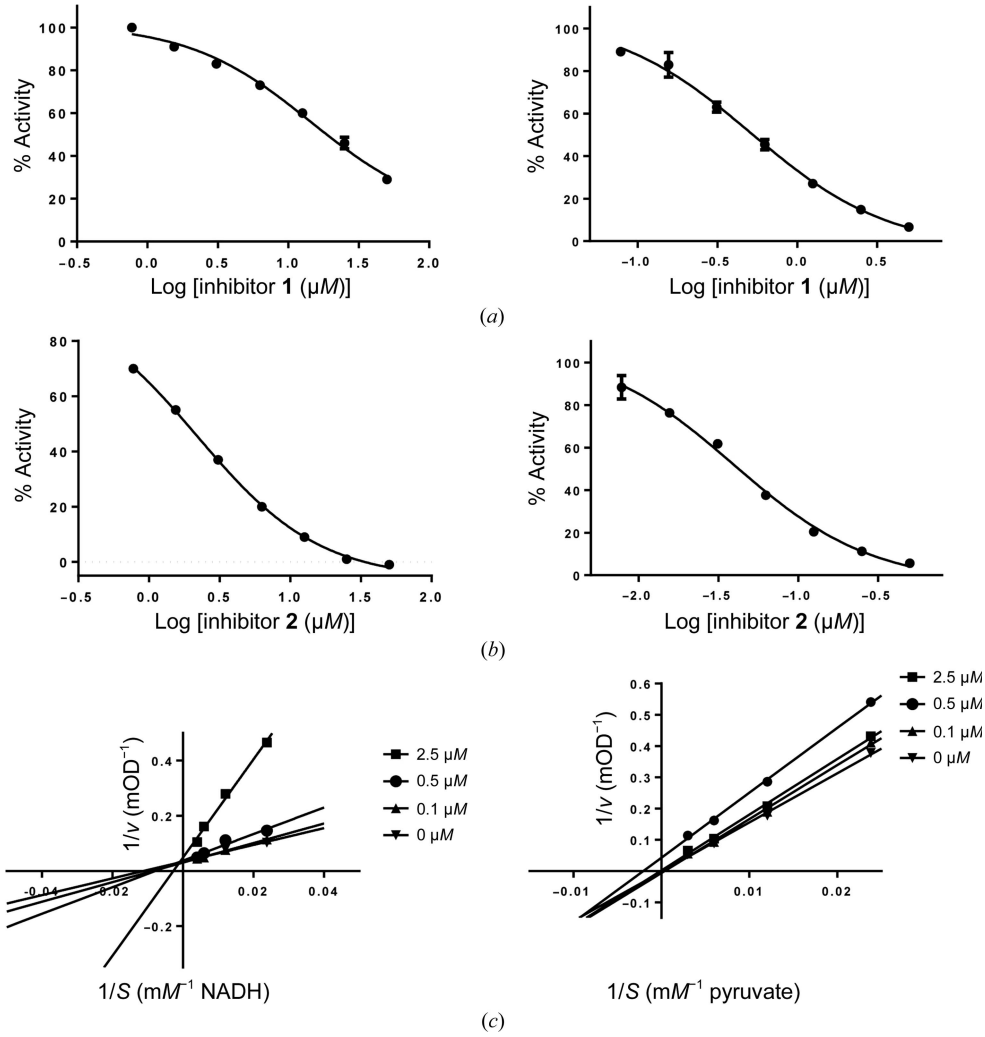

Figure 5
Quantification of LDHA inhibition by compounds **1** and **2**. (*a*) Compounds **1** and **2** demonstrate moderate inhibition of LDHA, as shown by an absorbance assay for the conversion of pyruvate to lactate. IC_{50} values are 14.4 $\pm$ 3.77 μM for compound **1** and 2.20 $\pm$ 0.15 μM for compound **2**. (*b*) Inhibition of the reverse reaction, conversion of lactate to pyuvate, was measured using a fluorescence assay, producing IC_{50} values of 0.51 $\pm$ 0.14 μM for compound **1** and 0.039 $\pm$ 0.007 μM for compound **2**. (*c*) Lineweaver–Burk plots for compound **2** to calculate K_i for NADH (K_i of 0.59 $\pm$ 0.09 μM) and pyruvate (K_i of 2.52 $\pm$ 0.21 μM).

for compound **2**: the inhibition is competitive with respect to NADH (K_i of 0.59 ± 0.09 µ*M*) and noncompetitive with respect to pyruvate (K_i of 2.52 ± 0.21 µ*M*) (Fig. 5*c*).

3.4. LDHA–inhibitor structures

Compounds **1** and **2** are shown in Fig. 6(*a*). These compounds are comprised of a central quinoline heterocycle with a dimethoxypyrimidine attached at C3 and an aminobenzoic acid at C6. They differ in the C7 constituent, which is an amide group in **1** and a sulfonamide group in **2**. LDHA–**1** and LDHA–**2** enzyme–inhibitor complex structures were obtained by soaking apo LDHA crystals in solution containing 20 m*M* compound **1** or **2** for 24 h, cryocooling the crystals and collecting X-ray diffraction data. LDHA–**1** and LDHA–**2** crystal structures were solved to resolutions of 3.2 and 3.0 Å, respectively. Although modest in resolution, the electron-density maps were refined using NCS and showed clear electron density to unambiguously fit the ligands in each of the eight molecules in the asymmetric unit. The LDHA–inhibitor complexes are highly similar to each other and to the open apo LDHA structure in terms of crystal packing and atomic coordinates. Compounds **1** and **2**, which are insoluble in aqueous solution, interact with LDHA *via* multiple hydrophobic contacts as well as *via* salt bridges and hydrogen bonds (Figs. 6*b* and 6*c*). Both ligands occupy the same binding site as kanamycin in the LDHA–oxl–kan structure and adopt V-shaped conformations and LDHA contacts similar to those of kanamycin (Figs. 6*b*, 6*c*, 6*d* and 4*b*). As with kanamycin, inhibitor binding involves minimal adjustment in LDHA. Only the Arg99 side-chain conformation is altered significantly: instead of moving out of the way as it does for kanamycin, the Arg99 guanidinium group stacks with the benzoate ring of **1** (Fig. 6*b*) and forms a salt bridge with the carboxyl group of the benzoate of **2** in some of the eight molecules in the asymmetric unit (Fig. 6*c*). In both structures the Arg99 backbone amide also contacts the benzoate carboxyl group *via* a hydrogen bond. Arg112 forms a salt bridge with this same carboxyl group in both inhibitor structures (Figs. 6*b* and 6*c*), but maintains its contacts with Glu104 as in the apo LDHA structure (see Fig. 4*d*). The

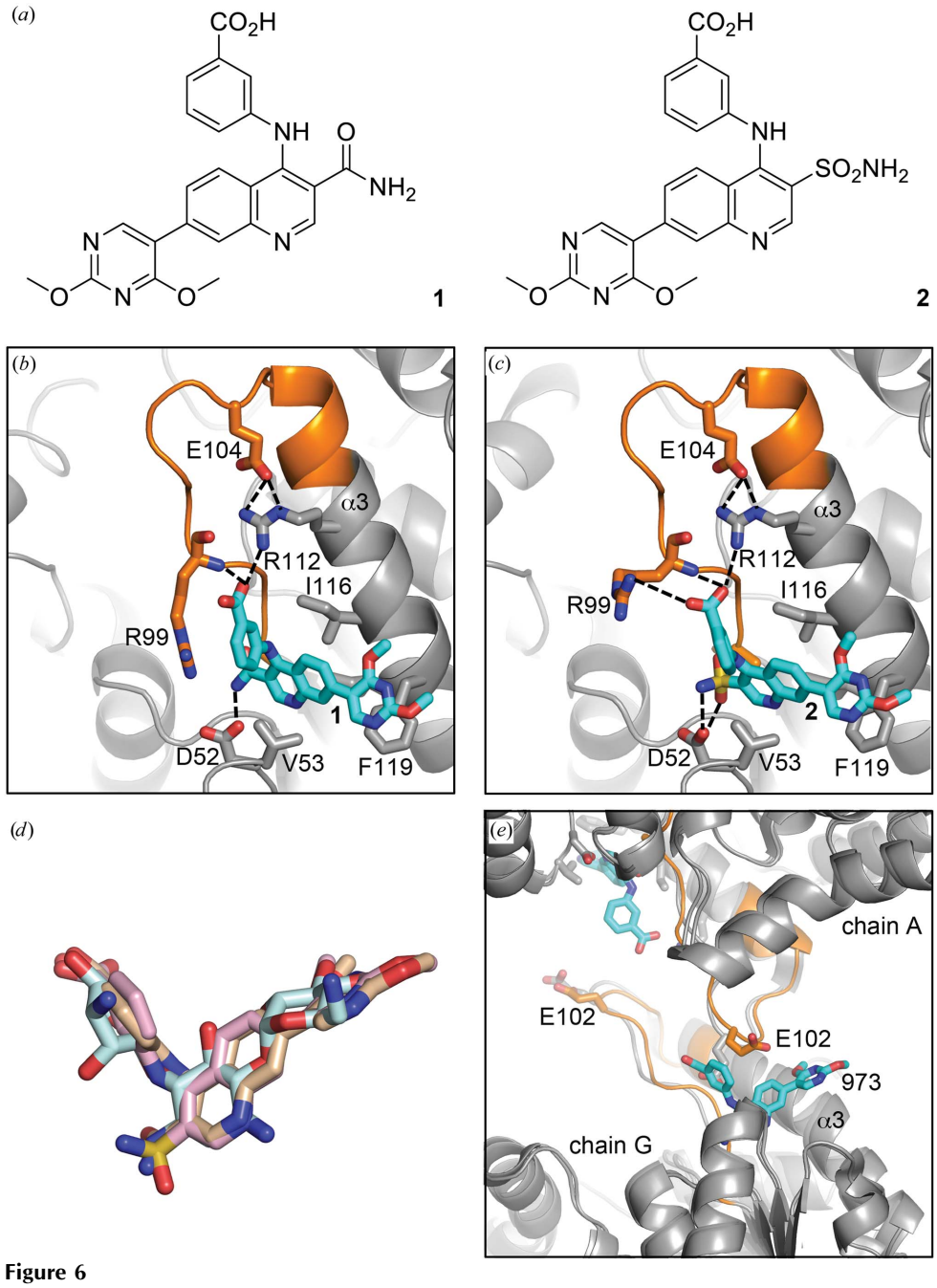

Figure 6
Structures of LDHA bound to inhibitors **1** and **2**. (*a*) Structures of **1** (3-{[3-carbamoyl-7-(2,4-dimethoxypyrimidine-5-yl)quinolin-4-yl]amino}benzoic acid) and **2** (3-{[7-(2,4-dimethoxypyrimidine-5-yl)-3-sulfamoylquinolin-4-yl]amino}benzoic acid). (*b*, *c*) Close-up of bound (*b*) **1** and (*c*) **2** showing interactions with LDHA. LDHA is shown in a grey cartoon representation with its active-site loop coloured orange. Interacting side chains are shown in stick representation, as are the inhibitors, with C atoms coloured cyan. N atoms are blue, O atoms are red and S atoms are yellow. (*d*) Superposition of kanamycin (cyan), **1** (yellow) and **2** (pink) as they are situated in the active site. (*e*) Superposition of chains *A* and *G* in the octameric apo LDHA and LDHA–**1** structures to show the change in the side-chain conformation of Glu102 in chain *A* when **1** is bound to chain *G*. A similar interaction is observed in the LDHA–**2** octamer. Colours are as described for (*b*) and (*c*).

central quinoline rings of the inhibitors are sandwiched between the hydrophobic side chains of Val53 and Ile116 and the dimethoxypyrimidines stack with Phe119. Asp52 hydrogen-bonds to the carbamoyl group in **1** and the sulfamoyl group in **2**. An additional contact, in this case between adjacent protein subunits in the octameric unit, occurs between Glu102 at the tip of the active site of chains *A* and *H* and the inhibitor in the adjacent chains *G* and *B*, respectively (Fig. 5*e*). The Glu102 side chain is rotated relative to its position in apo LDHA such that methylenes are inserted into the hydrophobic crook of the V-shaped inhibitors. Reciprocal interactions between chains *G* and *A* and chains *B* and *H* are not observed, as the chain *G* and *B* active-site loops do not insert into the active site of their partner chain.

4. Discussion

The human LDHA structures reported here, a new crystal form of apo LDHA, a ternary complex with the substrate inhibitor oxalate and NADH, a ternary structure with oxalate and kanamycin, and binary structures with bound inhibitors **1** and **2**, illustrate the ability of LDHA to bind to molecules with only minimal rearrangements in its side chains. Productive binding requires the presence of both pyruvate substrate and NADH co-substrate and closure of the active-site loop to exclude water molecules. In our oxalate/NADH-bound structures the active-site loop is closed, but this is not the case for all ternary structures (Read *et al.*, 2001; Swiderek *et al.*, 2009). Furthermore, closed active sites have been observed for apo LDH structures (Hogrefe *et al.*, 1987). These results imply a dynamic active-site loop that samples both conformations regardless of the occupancy of the active site. Compounds designed to restrict the movement/closure of this loop may prove to be effective inhibitors for LDHA.

While our ternary LDHA–oxl–NADH structures are closed, the single LDHA–oxl–kan structure is in an open conformation, as are the LDHA–inhibitor complexes. Kanamycin and compounds **1** and **2** all bind to the same site, the hydrophobic adenine-binding pocket at the exposed end of the active-site groove. While the presence of these compounds may restrict movement of the active-site loop, compounds **1** and **2** are likely to inhibit LDHA catalysis by preventing NADH from binding. This mechanism is supported by our competitive inhibition studies with compound **2**, which show that this inhibitor competes with NADH but not pyruvate. To our knowledge, kanamycin has not been reported as an LDHA inhibitor.

The molecular mimicry between kanamycin and inhibitors **1** and **2** is striking, with each molecule adopting a V-shaped conformation and binding to the same set of residues at the outermost portion of the active site. These inhibitors have limited solubility and bind to LDHA *via* mostly hydrophobic interactions. The adenine-binding site has been targeted by other inhibitors alone and in combination with substrate inhibitors (Kohlmann *et al.*, 2013; Ward *et al.*, 2012). Compared with these inhibitors, for the most part, compounds **1** and **2** possess equal or better potency and are generally more drug-like. The introduction of structural modifications to improve pharmacokinetic properties and address metabolic liabilities are the logical next steps to optimize these inhibitors.

Collectively, these structures further our understanding of LDH catalysis and the insights into their active-site binding provided by this study may aid the design of drug-like inhibitors that could selectivity target the aberrant glycolytic metabolism prevailing within many cancer cells and tumours.

We thank the staff at SSRL beamline 7-1 for assistance with remote data collection. This research was supported by CIHR grant MOP-125959 and NSERC ENGAGE grant EGP429365 to LC. KS was also supported in part by a Connect Canada industrial internship with Alectos Therapeutics Inc.

References

Abad-Zapatero, C., Griffith, J. P., Sussman, J. L. & Rossmann, M. G. (1987). *J. Mol. Biol.* **198**, 445–467.
Billiard, J. *et al.* (2013). *Cancer Metab.* **1**, 19.
Brünger, A. T., Adams, P. D., Clore, G. M., DeLano, W. L., Gros, P., Grosse-Kunstleve, R. W., Jiang, J.-S., Kuszewski, J., Nilges, M., Pannu, N. S., Read, R. J., Rice, L. M., Simonson, T. & Warren, G. L. (1998). *Acta Cryst.* D**54**, 905–921.
Carruthers, M. D., Tracy, E. N., Dickson, A. C., Ganser, K. B., Munson, R. S. & Bakaletz, L. O. (2012). *J. Bacteriol.* **194**, 1927–1933.
Chai, D., Colon, M., Dodson, C. S., Duffy, K. J. & Shaw, A. N. (2012). Patent WO 2012061557 A3.
Chen, V. B., Arendall, W. B., Headd, J. J., Keedy, D. A., Immormino, R. M., Kapral, G. J., Murray, L. W., Richardson, J. S. & Richardson, D. C. (2010). *Acta Cryst.* D**66**, 12–21.
Dempster, S., Harper, S., Moses, J. E. & Dreveny, I. (2014). *Acta Cryst.* D**70**, 1484–1490.
Dragovich, P. S. *et al.* (2013). *Bioorg. Med. Chem. Lett.* **23**, 3186–3194.
Dragovich, P. S. *et al.* (2014). *Bioorg. Med. Chem. Lett.* **24**, 3764–3771.
Dunn, C. R., Wilks, H. M., Halsall, D. J., Atkinson, T., Clarke, A. R., Muirhead, H. & Holbrook, J. J. (1991). *Philos. Trans. R. Soc. Lond. Ser. B Biol. Sci.* **332**, 177–184.
Emsley, P. & Cowtan, K. (2004). *Acta Cryst.* D**60**, 2126–2132.
Fantin, V. R., St-Pierre, J. & Leder, P. (2006). *Cancer Cell*, **9**, 425–434.
Fauber, B. P. *et al.* (2013). *Bioorg. Med. Chem. Lett.* **23**, 5533–5539.
Fiume, L., Manerba, M., Vettraino, M. & Di Stefano, G. (2010). *Pharmacology*, **86**, 157–162.
González, A., Moorhead, P., McPhillips, S. E., Song, J., Sharp, K., Taylor, J. R., Adams, P. D., Sauter, N. K. & Soltis, S. M. (2008). *J. Appl. Cryst.* **41**, 176–184.
Granchi, C., Calvaresi, E. C., Tuccinardi, T., Paterni, I., Macchia, M., Martinelli, A., Hergenrother, P. J. & Minutolo, F. (2013). *Org. Biomol. Chem.* **11**, 6588–6596.
Granchi, C., Roy, S., Giacomelli, C. *et al.* (2011). *J. Med. Chem.* **54**, 1599–1612.
Granchi, C., Roy, S., Mottinelli, M., Nardini, E., Campinoti, F., Tuccinardi, T., Lanza, M., Betti, L., Giannaccini, G., Lucacchini, A., Martinelli, A., Macchia, M. & Minutolo, F. (2011). *Bioorg. Med. Chem. Lett.* **21**, 7331–7336.
Hamanaka, R. B. & Chandel, N. S. (2012). *J. Exp. Med.* **209**, 211–215.
Hogrefe, H. H., Griffith, J. P., Rossmann, M. G. & Goldberg, E. (1987). *J. Biol. Chem.* **262**, 13155–13162.
Kabsch, W. (2010). *Acta Cryst.* D**66**, 125–132.
Kohlmann, A. *et al.* (2013). *J. Med. Chem.* **56**, 1023–1040.
Koukourakis, M. I., Giatromanolaki, A., Simopoulos, C., Polychronidis, A. & Sivridis, E. (2005). *Clin. Exp. Metastasis*, **22**, 25–30.
Koukourakis, M. I., Giatromanolaki, A., Sivridis, E., Bougioukas, G., Didilis, V., Gatter, K. C., Harris, A. L. & Tumour and Angiogenesis Research Group (2003). *Brit. J. Cancer*, **89**, 877–885.

Koukourakis, M. I., Pitiakoudis, M., Giatromanolaki, A., Tsarouha, A., Polychronidis, A., Sivridis, E. & Simopoulos, C. (2006). *Cancer Sci.* **97**, 1056–1060.
Laskowski, R. A., MacArthur, M. W., Moss, D. S. & Thornton, J. M. (1993). *J. Appl. Cryst.* **26**, 283–291.
Le, A., Cooper, C. R., Gouw, A. M., Dinavahi, R., Maitra, A., Deck, L. M., Royer, R. E., Vander Jagt, D. L., Semenza, G. L. & Dang, C. V. (2010). *Proc. Natl Acad. Sci. USA*, **107**, 2037–2042.
Luft, J. R., Collins, R. J., Fehrman, N. A., Lauricella, A. M., Veatch, C. K. & DeTitta, G. T. (2003). *J. Struct. Biol.* **142**, 170–179.
Manerba, M., Vettraino, M., Fiume, L., Di Stefano, G., Sartini, A., Giacomini, E., Buonfiglio, R., Roberti, M. & Recanatini, M. (2012). *ChemMedChem*, **7**, 311–317.
Matthews, B. W. (1968). *J. Mol. Biol.* **33**, 491–497.
McCoy, A. J., Grosse-Kunstleve, R. W., Adams, P. D., Winn, M. D., Storoni, L. C. & Read, R. J. (2007). *J. Appl. Cryst.* **40**, 658–674.
Murshudov, G. N., Skubák, P., Lebedev, A. A., Pannu, N. S., Steiner, R. A., Nicholls, R. A., Winn, M. D., Long, F. & Vagin, A. A. (2011). *Acta Cryst.* D**67**, 355–367.
Read, J. A., Winter, V. J., Eszes, C. M., Sessions, R. B. & Brady, R. L. (2001). *Proteins*, **43**, 175–185.
Sheng, S. L., Liu, J. J., Dai, Y. H., Sun, X. G., Xiong, X. P. & Huang, G. (2012). *FEBS J.* **279**, 3898–3910.
Swiderek, K., Panczakiewicz, A., Bujacz, A., Bujacz, G. & Paneth, P. (2009). *J. Phys. Chem. B*, **113**, 12782–12789.
Vander Heiden, M. G. (2011). *Nature Rev. Drug Discov.* **10**, 671–684.
Wang, Z.-Y., Loo, T. Y., Shen, J.-G., Wang, N., Wang, D.-M., Yang, D.-P., Mo, S.-L., Guan, X.-Y. & Chen, J.-P. (2012). *Breast Cancer Res. Treat.* **131**, 791–800.
Warburg, O. (1956). *Science*, **123**, 309–314.
Ward, R. A. *et al.* (2012). *J. Med. Chem.* **55**, 3285–3306.
Winn, M. D. *et al.* (2011). *Acta Cryst.* D**67**, 235–242.
Xie, H., Valera, V. A., Merino, M. J., Amato, A. M., Signoretti, S., Linehan, W. M., Sukhatme, V. P. & Seth, P. (2009). *Mol. Cancer Ther.* **8**, 626–635.
Xie, H. *et al.* (2014). *Cell Metab.* **19**, 795–809.
Yang, Y., Su, D., Zhao, L., Zhang, D., Xu, J., Wan, J., Fan, S. & Chen, M. (2014). *Oncotarget*, **5**.